Mitochondrial remodeling in hepatic differentiation and dedifferentiation

Wanet, Anaïs; Remacle, Noémie; Najar, Mehdi; Sokal, Etienne; Arnould, Thierry; Najimi, Mustapha; Renard, Patricia

Published in:
The international journal of Biochemistry & Cell biology

DOI:
10.1016/j.biocel.2014.07.015

Publication date:
2014

Document Version
Early version, also known as pre-print

The International Journal of Biochemistry & Cell Biology 54 (2014) 174–185

Contents lists available at ScienceDirect

The International Journal of Biochemistry & Cell Biology

journal homepage: www.elsevier.com/locate/biocel

Mitochondrial remodeling in hepatic differentiation and dedifferentiation

Anaïs Wanet[a], Noémie Remacle[a], Mehdi Najar[b], Etienne Sokal[c], Thierry Arnould[a], Mustapha Najimi[c], Patricia Renard[a,*]

[a] Laboratory of Biochemistry and Cell Biology (URBC), NAmur Research Institute for LIfe Sciences (NARILIS), University of Namur (UNamur), 61 rue de Bruxelles, 5000 Namur, Belgium
[b] Laboratory of Clinical Cell Therapy, Institut Jules Bordet, Université Libre de Bruxelles (ULB), Brussels, Belgium
[c] Université Catholique de Louvain, Institut de Recherche Clinique et Expérimentale (IREC), Laboratory of Pediatric Hepatology and Cell Therapy, Brussels, Belgium

ARTICLE INFO

Article history:
Received 23 January 2014
Received in revised form 20 June 2014
Accepted 22 July 2014
Available online 30 July 2014

Keywords:
Oxidative phosphorylation
Hepatocytes
Mesenchymal stromal cells
Mitochondrial turnover
Cell (de)differentiation

ABSTRACT

Mitochondrial biogenesis and metabolism have recently emerged as important actors of stemness and differentiation. On the one hand, the differentiation of stem cells is associated with an induction of mitochondrial biogenesis and a shift from glycolysis toward oxidative phosphorylations (OXPHOS). In addition, interfering with mitochondrial biogenesis or function impacts stem cell differentiation. On the other hand, some inverse changes in mitochondrial abundance and function are observed during the reprogramming of somatic cells into induced pluripotent stem cells (iPSCs). Yet although great promises in cell therapy might generate better knowledge of the mechanisms regulating the stemness and differentiation of somatic stem cells (SSCs)—which are preferred over embryonic stem cells (ESCs) and iPSCs because of ethical and safety considerations—little interest was given to the study of their mitochondria. This study provides a detailed characterization of the mitochondrial biogenesis occurring during the hepatogenic differentiation of bone marrow-mesenchymal stem cells (BM-MSCs). During the hepatogenic differentiation of BM-MSCs, an increased abundance of mitochondrial DNA (mtDNA) is observed, as well as an increased expression of several mitochondrial proteins and biogenesis regulators, concomitant with increased OXPHOS activity, capacity, and efficiency. In addition, opposite changes in mitochondrial morphology and in the abundance of several OXPHOS subunits were found during the spontaneous dedifferentiation of primary hepatocytes. These data support reverse mitochondrial changes in a different context from genetically-engineered reprogramming. They argue in favor of a mitochondrial involvement in hepatic differentiation and dedifferentiation.

Abbreviations: α1AT, α-1-antitrypsin; BM-MSCs, bone-marrow mesenchymal stem cells; COX1, subunit I of the cytochrome c oxidase; COX2, subunit II of the cytochrome c oxidase; COX4, subunit IV of the cytochrome c oxidase; DRP1, dynamin-related protein 1; ECAR, extracellular acidification rate; ERR, estrogen-related receptors; ESCs, embryonic stem cells; FCCP, carbonyl cyanide 4-(trifluoromethoxy)phenylhydrazone; G6PC, glucose-6-phosphatase catalytic subunit; iPSCs, induced pluripotent stem cells; mtDNA, mitochondrial DNA; ND2, NADH dehydrogenase subunit 2; NRF-1 and-2, nuclear respiratory factor 1 and 2; OCR, oxygen consumption rate; OTC, ornithine transcarbamylase; nDNA, nuclear DNA; OXPHOS, oxidative phosphorylation; PEPCK1, phosphoenolpyruvate carboxykinase 1; PGC-1, PPAR gamma coactivator 1; PPAR, peroxisome proliferator-activated receptor; PPIE, peptidyl-prolyl cis-trans isomerase E; PRC, PGC-1-related coactivator; SSCs, somatic stem cells; TAT, tyrosine aminotransferase; TDO2, tryptophan 2,3-dioxygenase; TFs, transcription factors; TFAM, mitochondrial transcription factor A.

* Corresponding author. Laboratory of Biochemistry and Cell Biology (URBC), NAmur Research Institute for LIfe Sciences (NARILIS), University of Namur (UNamur), 61 rue de Bruxelles, 5000 Namur, Belgium, Tel.: +32 0 81 72 41 28; fax: +32 0 81 72 41 35.
E-mail addresses: anais.wanet@unamur.be (A. Wanet), noemie.remacle@hotmail.fr (N. Remacle), Mehdi.Najar@ulb.ac.be (M. Najar), etienne.sokal@uclouvain.be (E. Sokal), thierry.arnould@unamur.be (T. Arnould), mustapha.najimi@uclouvain.be (M. Najimi), patsy.renard@unamur.be (P. Renard).

http://dx.doi.org/10.1016/j.biocel.2014.07.015
1357-2725/

1. Introduction

Depending on physiologic and cellular cues, mitochondria can display differences in their abundance, morphology and functions. Mitochondrial biogenesis is a complex process involving lipid membrane formation, mitochondrial DNA (mtDNA) replication and transcription, and coordinated synthesis of mitochondrial proteins encoded by both nuclear and mitochondrial genomes. The coordination between the nuclear and mitochondrial genomes is achieved through the expression of nucleus-encoded mitochondrial proteins which control mtDNA replication and transcription, such as the mitochondrial transcription factor A (TFAM). In the nucleus, the expression of mitochondrial genes is controlled by a limited number of transcription factors (TFs), including NRF-1 and -2 (nuclear respiratory factors 1 and 2), PPARs (peroxisome proliferator-activated receptors α, β/δ, and γ) and ERRs (estrogen-related receptors α, β, and γ). (Interested readers can refer to (Hock and Kralli, 2009) for a detailed review of the involvement of these TFs in mitochondrial biogenesis). The activity of these TFs is itself controlled by the PGC-1 (PPAR gamma coactivator 1) family of coactivators: PGC-1α; PGC-1β; and PRC (PGC-1-related coactivator) (Hock and Kralli, 2009). Among these, the best described is PGC-1α, a protein considered to be the master regulator of mitochondrial biogenesis and function (Fernandez-Marcos and Auwerx, 2011).

A number of recent studies evidenced an enhanced mitochondrial biogenesis in various stem cell differentiation models (Chen et al., 2012, Xu et al., 2013). In ESCs, the mitochondrial phenotype has been described as "immature," consisting of few mitochondria, containing poorly developed cristae, and displaying a perinuclear location (Cho et al., 2006, Lonergan et al., 2007, St John et al., 2005). While these cells mainly rely on glycolysis for their energy production, differentiating cells display an increased mitochondrial mass and mtDNA abundance, a more developed mitochondrial network, and a shift toward OXPHOS to meet their energy demands (Chung et al., 2010, Facucho-Oliveira et al., 2007, Lonergan, Bavister, 2007, Prigione et al., 2010, Suhr et al., 2010). In addition, the use of molecules promoting or inhibiting mitochondrial biogenesis or function, or interfering with the expression of mitochondrial biogenesis regulators or proteins involved in mitochondrial function, has been demonstrated to impact stemness and cell differentiation (Huang et al., 2011, Tormos et al., 2011, Xu et al., 2013). For instance, the attenuation of mitochondrial function using carbonyl cyanide *m*-chlorophenylhydrazone (CCCP) in ESCs results in increased transcriptional levels of the pluripotency markers Sox2, Oct4, and Nanog, and in the repression of transcriptional programs associated with lineage differentiation (Mandal et al., 2011). Conversely, the reprogramming of somatic cells into iPSCs is accompanied by inverse modifications, in a process called "mitochondrial rejuvenation" (Folmes et al., 2011, Prigione, Fauler, 2010, Suhr, Chang, 2010, Varum et al., 2011). These data have led to the hypothesis that transitions in mitochondrial metabolism regulate, or are regulated by, differentiation and reprogramming events.

In order to better appreciate the involvement of mitochondria in differentiation processes, two main points remain to be addressed. On the one hand, due to the lack of an extensive characterization of the mitochondria in the different stem cell differentiation models previously studied, it is currently unclear if the mitochondrial biogenesis process always involves an increase in all or some of the constituents of mitochondria (membrane, protein and mtDNA) and if it systematically results in increased mitochondrial activity. In addition, the kinetics of the mitochondrial biogenesis has not been addressed in most studies, and it remains unclear when, and for how long, the mitochondrial biogenesis is induced. On the other hand, while most studies of mitochondrial biogenesis in stemness and differentiation have been performed on ESCs and iPSCs, few studies report an enhanced mitochondrial biogenesis during the differentiation of SSCs such as mesenchymal stem cells (MSCs) (Chen et al., 2008, Palomaki et al., 2013, Pietila et al., 2012, Tormos, Anso, 2011). If the mitochondrial biogenesis represents a hallmark of all types of stem cell differentiation processes therefore remains to be demonstrated. Although not as pluripotent as ESCs, SSCs offer several advantages over ESCs/iPSCs in cell therapy, such as better safety and fewer ethical concerns. Among SSCs, MSCs can differentiate into multiple cell types, including hepatocytes (Banas et al., 2007, Mosna et al., 2010). Interestingly, hepatocytes display a much higher expression of several mitochondrial OXPHOS subunits (Suppl. Fig. 1) than BM-MSCs, suggesting that a strong mitochondrial biogenesis might be associated with their differentiation.

Primary hepatocytes, however, cannot be maintained in culture in a fully differentiated and highly metabolic state. Hepatocytes are subject to a rapid dedifferentiation process during *in vitro* culture. This process is initiated during their isolation, and is characterized by: rapid loss of hepatic gene expression, polarity, and activity; re-entry into the cell cycle; and upregulation of cytoskeleton and mesenchymal proteins such as vimentin (Elaut et al., 2006, Meyer et al., 2013). Improving our understanding of the mechanisms involved in hepatocyte dedifferentiation, and eventually counteracting them, could thus lead to many important applications such as pharmacological testing. The demonstration of an involvement of mitochondria in hepatic differentiation and dedifferentiation processes might therefore be used as a starting point for studies aimed to improve/limit hepatocyte differentiation/dedifferentiation.

In this study, we provide a kinetic and detailed characterization of the mitochondrial biogenesis initiated during the hepatogenic differentiation of BM-MSCs. We provide evidence for inverse mitochondrial changes during the spontaneous dedifferentiation of hepatocytes. We initially found evidence for an induction of mitochondrial and mtDNA abundance and an increased expression of several mitochondrial proteins and mitochondrial biogenesis regulators, concomitant with an increased oxidative activity, during the early hepatogenic differentiation of BM-MSCs. In contrast, during primary hepatocyte dedifferentiation we found a reduction of several mitochondrial proteins involved in OXPHOS. Furthermore, while a fission of the mitochondrial network was observed in the differentiation model, a trend toward an increased fusion was observed during hepatocyte dedifferentiation. These data demonstrate the existence of opposite changes in mitochondrial morphology and function between the hepatic differentiation and hepatocyte dedifferentiation models. They further support the involvement of mitochondria in stemness and cell differentiation.

2. Material and methods

2.1. Ethical guidelines

This study was approved by the local ethics committee of the Jules Bordet Institute (Belgium) for obtaining human BM-MSCs after informed consent from donors. The use of human liver tissue for research was approved by the ethical committee of St-Luc Hospital and of the Université Catholique de Louvain, Belgium. Primary hepatocytes were obtained from the Hepatocyte and Liver Stem cell Tissue Bank of Cliniques St Luc, acting under the agreement of the Belgian Ministry of Health.

2.2. Cell culture and differentiation

Cultures of human BM-MSCs were established as previously described (Najar et al., 2013) from 4 different healthy donors (aged 2–22 years old). BM-MSCs were expanded in Dulbecco's Modified Eagle Medium low glucose (DMEM-LG) supplemented by 1%

penicillin streptomycin mixture (Life Technologies, Carlsbad, CA, USA) and 10% fetal bovine serum (FBS, PAA/GE Healthcare, Piscataway, NJ, USA). Prior to the hepatogenic induction, BM-MSCs were seeded on type-1 collagen (BD Biosciences, San Jose, CA) coated dishes and expanded till 95% confluency (« day 0 »). Hepatogenic induction was carried out by incubating BM-MSCs in Iscove's Modified Dulbecco's Medium (IMDM, Life Technologies) containing 1% penicillin streptomycin mixture and supplemented with 20 ng/ml EGF (PeproTech, Rocky Hill, NJ, USA) and 10 ng/ml FGF-2 (PeproTech) for 48 h and then with 10 ng/ml FGF-2, 20 ng/ml HGF (PeproTech), 0,61 mg/ml nicotinamide (Sigma–Aldrich, Saint-Louis, MO, USA) and insulin-transferrin-selenium (ITS) mixture 1X (Life Technologies) for 10 days. Cells were then treated with a hepatogenic maturation cocktail containing 20 ng/ml oncostatin M (OSM) (PeproTech), 1 μM dexamethasone (Sigma–Aldrich) and ITS for 10 days. Undifferentiated BM-MSCs were maintained in IMDM supplemented with 1% FBS. All experiments were performed at passage 5–6.

Primary human hepatocytes were isolated from 3 healthy cadaveric donors (4 days, 27 and 48 years old) using a classic two-step perfusion technique as previously described (Najimi et al., 2007). Hepatocytes were seeded on type-1 collagen coated dishes and maintained in Williams'E medium (Life Technologies) supplemented with 1% penicillin-streptomycin, 10% FBS (Life Technologies), 1.275 μM dexamethasone (Aacidexam) and 1.66 10^{-5} U/ml insulin (Lilly Benelux SA, Brussels, Belgium) for an 8-day dedifferentiation period.

All cells were maintained at 37 °C in a humidified atmosphere containing 5% CO_2.

2.3. Periodic acid Schiff staining

Cells were seeded on coverslips, fixed with 4% paraformaldehyde for 20 min and then stained using the periodic acid-schiff staining system (Sigma–Aldrich). Briefly, cells were incubated with 1% periodic acid for 10 min, rinsed several times with deionized water, incubated with Schiff's reagent for 15 min, rinsed several times with tap water and then observed under a contrast-phase light microscope.

2.4. Nucleoids and mitochondrial network visualization and analysis

To analyze the mitochondrial network morphology, expanded, differentiated and undifferentiated BM-MSCs seeded on coverslips were stained with 100 nM Mitotracker® Green FM (Molecular Probes, Life Technologies) for 30 min at 37 °C and with CellMask™ Orange (Molecular Probes, Life Technologies) at a dilution 1:4000 during the last 5 min. Live cells were observed using confocal microscopy (TCS SP5 II, Leica Microsystems, Wetzlar, Germany). Dedifferentiating hepatocytes seeded on coverslips were fixed with 4% paraformaldehyde for 20 min, permeabilized for 5 min with PBS-1% Triton X-100, and then incubated for 2 h with anti-TOM20 antibody (BD Bioscience #612278) diluted in PBS -1% BSA (1:100). Cells were then incubated for 1 h with an Alexa-labeled secondary antibody (Molecular Probes) (1:1000) and observed by confocal microscopy. The length and branching status of the mitochondrial network was determined by calculating the aspect ratio (AR) and end points/branch points ratio of mitochondrial particles in the entire cell sections using the Image J software according to De Vos and Sheetz (De Vos and Sheetz, 2007). To analyze nucleoids as well as the percentage of the cytoplasmic area occupied by mitochondria, cells were seeded on coverslips, fixed with 4% paraformaldehyde for 20 min, permeabilized for 5 min with PBS-1% Triton X-100, and then incubated for 2 h with an anti-TOM20 antibody (SC-11415, 1:200) (for mitochondria staining) and an anti-DNA antibody (Progen AC-30-10, 1:10) (for nucleoid staining) or an anti-β-catenin antibody (BD610153, 1:100) (for cytoplasm staining) diluted in PBS -1% BSA. Cells were then incubated for 1 h with Alexa-labeled secondary antibodies (Molecular Probes) (1:1000) and observed by confocal microscopy. The number of nucleoids per cell section, as well as the area occupied by mitochondrial and nucleoid or cytoplasmic stainings were calculated using the ImageJ software.

2.5. Determination of the relative abundance of mtDNA

Total DNA was isolated using the Wizard Genomic DNA purification system (Promega, Fitchburg, MI, USA). The relative mtDNA copy number was estimated by quantitative real-time PCR (qPCR) using primers for the mitochondrial gene NADH dehydrogenase subunit 2 (ND2) and normalized to the genomic DNA by using primers for the beclin gene (Table A1). Reactions were performed using SYBR Green PCR Master mix (Roche) and an ABI 7900 HT Fast Real Time PCR System (Applied Biosystems, Life Technologies). Results are expressed relative to expanding BM-MSCs.

2.6. Real-time RT-qPCR analysis

Total RNA was isolated using the RNeasy Mini kit and Qiacube (Qiagen, Venlo, The Netherlands) and reverse-transcribed using the cDNA first strand synthesis kit (Roche Applied Science, Pensberg, Germany). RT-qPCR was performed using SYBR Green PCR Master mix (Roche), the primers listed in Table A1 and an ABI 7900 HT Fast Real Time PCR System. The mRNA abundance of glucose-6-phosphatase catalytic subunit (G6PC), phosphoenolpyruvate carboxykinase 1 (PEPCK1), ornithine transcarbamylase (OTC) and tyrosine aminotransferase (TAT) was determined using a PCR array from Qiagen according to the manufacturer's instructions. All results were normalized to the mRNA abundance of the peptidylprolyl cis-trans isomerase E (PPIE), and are expressed relative to expanding BM-MSCs or hepatocytes at « 0 h ».

2.7. Western blot analysis

Total cell protein lysates were obtained using a buffer containing 7 M urea, 2 M thiourea, 1% CHAPS, 1% ASB14, 1% SDS, 30 mM Tris, pH 8.5 supplemented with Complete Protease Inhibitor Cocktail (Roche) and 4% phosphatase inhibitor cocktail (25 mM Na_3VO_4, 250 mM 4-nitrophenylphosphate, 250 mM glycerophosphate, 125 mM NaF). An amount of 25 μg of proteins was resolved on 12% (PPARγ) or 4–15% (other proteins) Mini-PROTEAN TGX precast gels (Biorad, Hercules, CA, USA). Western blotting analysis was performed using the primary antibodies listed in Table A2, secondary antibodies coupled to Infrared dyes [(1:5000 (anti-goat IgG) or 1:10 000 (anti-mouse or anti-rabbit IgG), Li-Cor Biosciences, Lincoln, NE, USA)] and detection by infrared fluorescence (Odyssey scanner, Li-Cor Biosciences). The fluorescence signal intensity of the detected bands was calculated using the Odyssey V3.0 application software, normalized to the one of Histone 3 (used as loading control). Results are expressed relative to expanding BM-MSCs or to dedifferentiating hepatocytes at 18 h.

2.8. Respiration assays

The extracellular flux analyzer XF96 (Seahorse Biosience, North Billerica, MA, USA) was used to measure the oxygen consumption rate (OCR) and extracellular acidification rate (ECAR) at the end of the hepatogenic induction step (day 12). The necessity to perform the analysis on the same day excluded the possibility to analyze the respiration of corresponding expanding BM-MSCs. The day prior to the assay, cells were seeded at a density of 20,000 cells/well. A XF

Table A1
Sequences of primers used in qPCR.

Genes	Forward primer (5′ → 3′)	Reverse primer (5′ → 3′)
Albumin	TGTTGCATGAGAAAACGCCA	GTCGCCTGTTCACCAAGGAT
ATP5A1 (ATP synthase α subunit 1)	TCGGTTCTGACCTCGATGCT	ACCCGCATAGATAACAGCCAC
Beclin (nuclear gene)	CCCTCATCACAGGGCTCTCTCCA	GGGACTGTAGGCTGGGAACTATGC
COX1 (cytochrome c oxidase, subunit 1)	CCTGACTGGCATTGTATTAGC	TTTTGGCGTAGGTTTGGTCT
COX2 (cytochrome c oxidase, subunit 2)	AGATGCAATTCCCGGACGT	CATGAAACTGTGGTTTGCTCC
COX4i1 (cytochrome c oxidase, subunit 4 isoform 1)	ACCGCGCTCGTTATCATGTG	CATGTCCAGCATCCTCTTGGT
mtHSP70 (mitochondrial heat shock protein 70)	CTGAAGAAGACCGGCGAAAGA	AGCTTGTTGCACTCATCAGCA
ND2 (NADH dehydrogenase, subunit 2 (mitochondrial gene))	TGTTGGTTATACCCTTCCCGTACTA	CCTGCAAAGATGGTAGAGTAGATGA
OTC (ornithine transcarbamoylase)	GCGAAATTCGGAATGCACCTT	GCTCTGCCAACTTGGTTACAC
PGC-1α (peroxisome proliferator-activated receptor gamma, coactivator 1 alpha)	TCCTTTCTCTCGCCCAACACGATCT	GCATCCGACAGGACAAACAGTGGA
PGC-1β (peroxisome proliferator-activated receptor gamma, coactivator 1 beta)	AGCATTGGCTTGGAGCATCT	AGGGCTCGTGTTGGTTTCAA
PPARγ (peroxisome proliferator-activated receptor gamma)	GATGACAGCGACTTGGCAAT	AGGGCTTGTAGCAGGTTGTC
PPIE (Peptidyl-prolyl cis-trans isomerase E)	CCGCTCTTGACCCTGCATAT	TCCAAGCAGACCCTGAGGAA
Slug	ATTCGGACCCACACATTACCT	CTGTTGCAGTGAGGGCAAGAA
Sox9	CACACAGCTCACTCGACCTTG	TTCTTCGGTTATTTTTAGGATCATCTC
TDO2 (tryptophan 2,3-dioxygenase)	GAGGAACAGGTGGCTGAATTT	GCTCCCTGAAGTGCTCTGTA
Vimentin	GAGGCTGCCAACCGGAACAATG	TCCATTTCACGCATCTGGCGTTC
α1AT (alpha-1 antitrypsin)	GGGTCAACTGGGCATCACTAA	CCCTTTCTCGTCGATGGTCA

cell mito stress test (Seahorse Bioscience) was performed according to the manufacturer's instructions and using the following chemical concentrations: 1 μM oligomycin, 0.5 μM carbonyl cyanide 4-(trifluoromethoxy)phenylhydrazone (FCCP), 1 μM antimycin A and 1 μM rotenone. Once OCR and ECAR measurements were performed, cells were lysed in 0.5 N NaOH and OCR and ECAR measurements were normalized to the protein content of the well. Basal respiration was calculated by subtracting the non-mitochondrial oxygen consumption (OCR following the addition of both antimycin A and rotenone) to the basal OCR. ATP coupling efficiency is calculated by subtracting the non-mitochondrial oxygen consumption from the OCR following oligomycin addition and is expressed as a percentage of the basal respiration. Spare respiratory capacity is calculated by subtracting the non-mitochondrial oxygen consumption from the OCR following FCCP addition and is expressed as a percentage of the basal respiration. For each condition and each donor, 4–12 technical replicates were performed.

2.9. Statistical analyses

Depending on the data to compare, one-tailed *T*-test (Suppl. Fig. 1(A)), one way analysis of variance (Fig. 7(B)) or one way (Fig. 1(B), Fig. 2(B), Fig. 4(B), Fig. 6, Fig. 7(C))/two ways (Fig. 3 (A)–(C), Fig. 4(A), Fig. 5(A), Fig. 5(B), Suppl. Fig. 2, Suppl. Fig. 3) repeated measure ANOVA tests were performed, assuming data normal distribution. When equal variance test failed, Friedman repeated measures analysis of variance on ranks was performed instead (Fig. 4(A) for COX4 protein abundance). To identify the significantly different groups, pairwise multiple comparisons using the Student-Newman-Keuls method were performed (* or #, $p < 0.05$; ** or ##, $p < 0.01$; *** or ###, $p < 0.001$) (*, comparisons between different time points; #, comparisons between Diff and Undiff at a particular time point). All statistical analyses were done using the SigmaStat 3.2 software (Systat, San Jose, CA, USA).

3. Results

3.1. The in vitro hepatogenic differentiation of BM-MSCs

BM-MSCs were submitted to a hepatogenic differentiation protocol that consists of a sequential incubation with growth factors, cytokines and cofactors (Fig. 1 (A)). The cells obtained during or at the end of this process, defined as differentiated cells (Diff), were compared with undifferentiated cells (Undiff) cultured over the same period in a control medium, as well as with expanding BM-MSCs (Exp) from the corresponding passage. These two control conditions were analyzed to observe the changes due to cell differentiation *per se* or to the prolonged *in vitro* culture period.

The efficiency of hepatogenic differentiation of BM-MSCs was evaluated at the morphologic, genetic and functional levels. At the end of the last maturation step, an increased mRNA abundance of several hepatic markers such as albumin, α-1-antitrypsin (α1AT) or tryptophan 2,3-dioxygenase (TDO2) ($p = 0.053$) was noticed. At the same time, the abundance of the pluripotent marker Sox9 mRNA was suppressed (Fig. 1 (B)).

While relatively heterogeneous, differentiated cells also develop an increased ability to store glycogen as evidenced by periodic acid–Schiff (PAS) staining (Fig. 1 (C)). On these micrographs, one can observe the acquisition of the typical hepatocyte-like polygonal shape of the differentiated cells.

3.2. The mitochondrial network of BM-MSCs undergoes morphological changes during hepatogenic differentiation

Although the globular shape and perinuclear localization of mitochondria in ESCs and iPSCs has been regarded as a potential marker of pluripotency (Lonergan, Bavister, 2007), it is not clearly established if the morphology of the mitochondrial network is pluripotency-dependent or stem cell specific. Staining of

Table A2
Antibodies used for Western-blotting applications.

Target	Manufacturer	Reference	Dilution factor
Histone 3	Cell Signaling Technology (Danvers, MA, USA)	#4499	1:5000
COX1 (Cytochrome c oxidase, subunit 1)	Abcam (Cambridge, UK)	ab14705	1:2000
COX2 (Cytochrome c oxidase, subunit 2)	Abcam (Cambridge, UK)	ab110258	1:2000
COX4 (Cytochrome c oxidase, subunit 3)	Life Technologies (Carlsbad, CA, USA)	A21348	1:500
ATP synthase α	Life Technologies (Carlsbad, CA, USA)	A21350	1:1000
mtHSP70 (mitochondrial heat shock protein 70)	Enzo Life Sciences (Farmingdale, NY, USA)	ALX-804-077	1:1000
PPARγ (peroxisome proliferator-activated receptor gamma)	Santa Cruz Biotechnology (Dallas, TX, USA)	SC-7196	1:500
PGC-1α (peroxisome proliferator-activated receptor gamma, coactivator 1 alpha)	Santa Cruz Biotechnology (Dallas, TX, USA)	SC-13067	1:500

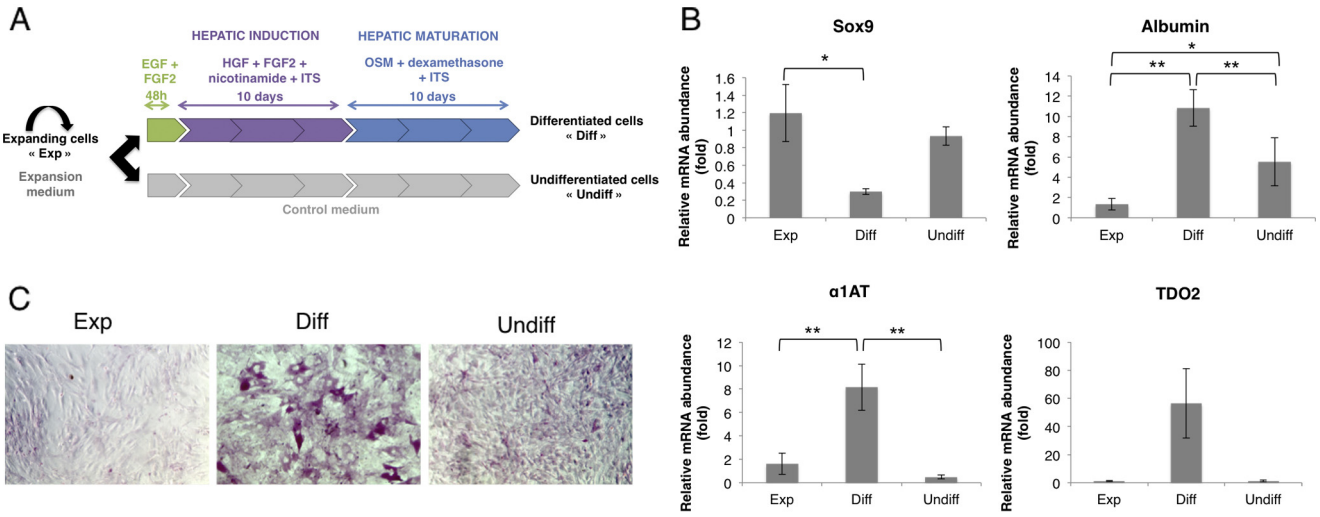

Fig. 1. The hepatogenic differentiation of BM-MSCs results in the acquisition of hepatic features. (A): Representation of the hepatogenic differentiation protocol and experimental conditions. (B): mRNA abundance of several pluripotency (Sox9) and hepatic markers (Albumin, α-1-antitrypsin (α1AT), tryptophan 2,3-dioxygenase (TDO2)) in expanding, differentiated and undifferentiated BM-MSCs determined using RT-qPCR. Data are presented as mean ± SEM ($n = 4$ independent donor cells). (C): Periodic-acid Schiff staining illustrating the ability of some differentiated cells to store glycogen.

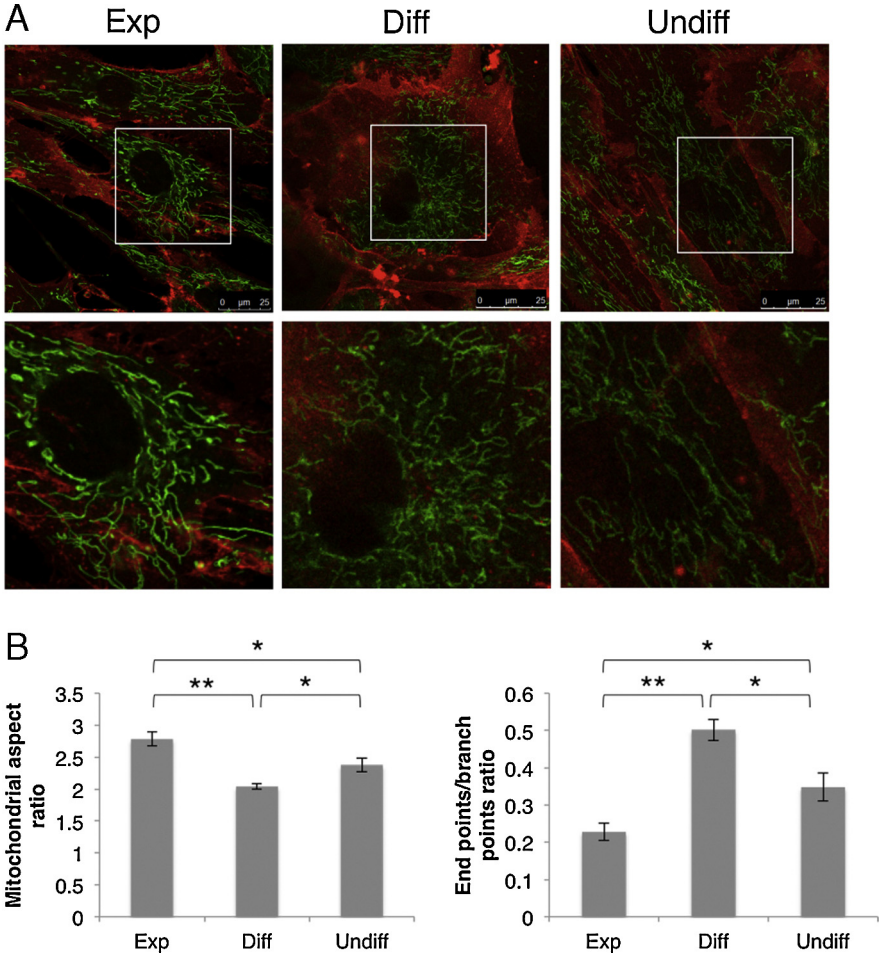

Fig. 2. The hepatogenic differentiation of BM-MSCs is accompanied by changes in the mitochondrial network morphology. (A): Living expanding, differentiated and undifferentiated BM-MSCs were stained with mitotracker green® FM (green) and cell Mask™ Orange (red) and observed using confocal microscopy. (B): Two parameters of the mitochondrial network morphology, the aspect ratio and end points/branch points ratio were analyzed for 10 cells for each condition and for 4 different donors. Data were first averaged for the 10 cells obtained for each donor in each condition and are presented as mean ± SEM of the data obtained for the 4 independent donors.

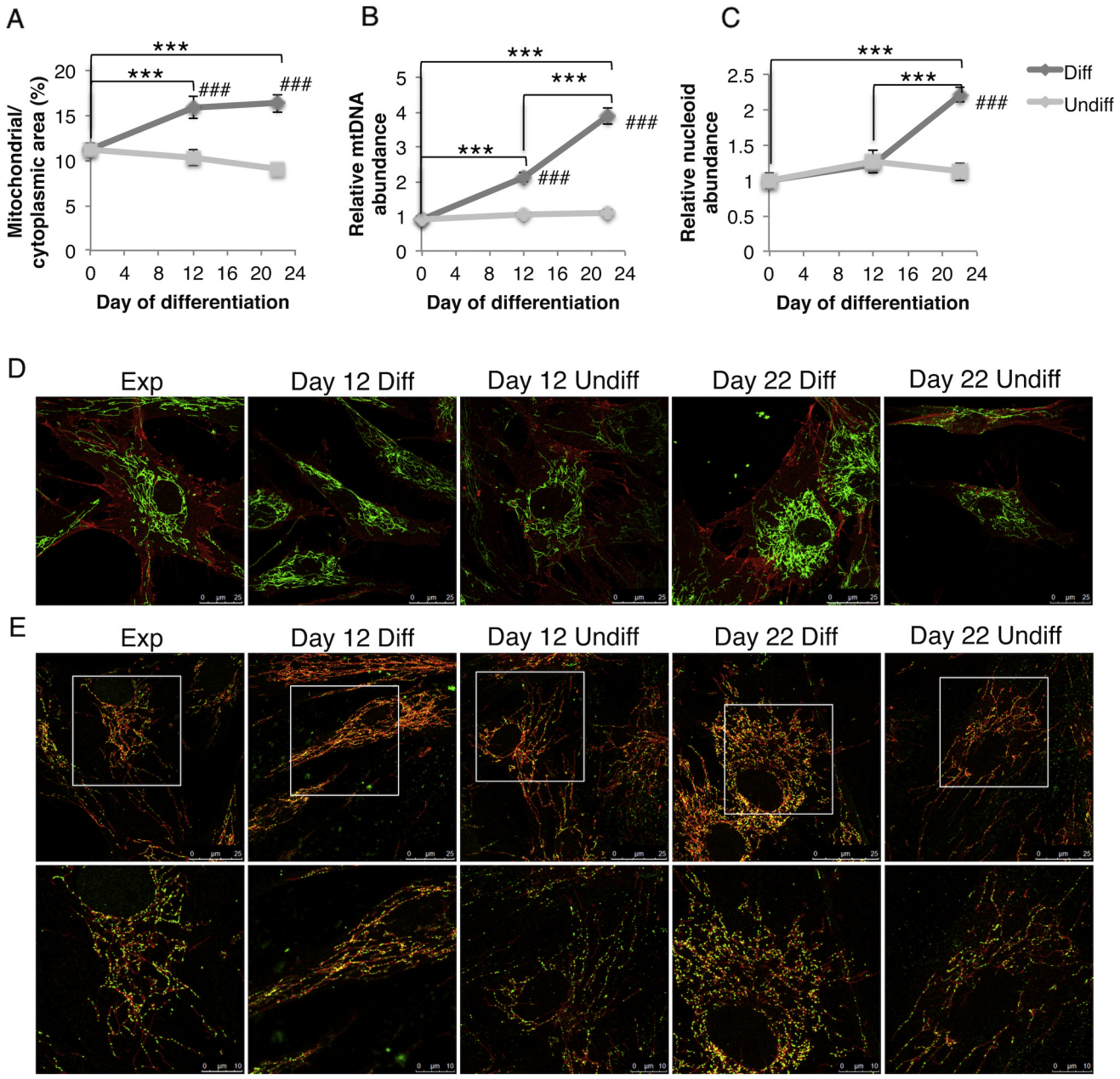

Fig. 3. An increase in mitochondria and mtDNA abundance is observed during the hepatogenic differentiation of BM-MSCs. (A): The percentage of the cytoplasmic area (visualized by β-catenin immunostaining, see Fig. 3 (D)) occupied by mitochondria (visualized by TOM20 immunostaining, see Fig. 3 (D)) was determined for 10 cells per donor for each condition and for 4 different donors. Data were first averaged for the 10 cells obtained for each donor in each condition and are presented as mean ± SEM of the data obtained for the 4 independent donors. (B): Relative abundance of the mtDNA content determined by quantitative PCR. Data are presented as mean ± SEM ($n = 4$ independent donor cells). (C): The number of nucleoids per cell section (determined by nucleoid immunostaining, see Fig. 3 (E)) was calculated for 10 cells per donor for each condition and for 4 different donors. Data were first averaged for the 10 cells obtained for each donor in each condition and are presented as mean ± SEM of the data obtained for the 4 independent donors. (D): Immunofluorescence staining of mitochondria (using an anti-TOM20 antibody, in green) and cytoplasm (using an anti-β-catenin antibody, in red) visualized by confocal microscopy. (E): Immunofluorescence staining of nucleoids (using an anti-DNA antibody, in green) and mitochondria (using an anti-TOM20 antibody, in red) visualized by confocal microscopy.

the mitochondrial network of BM-MSCs with MitoTracker® Green (a probe that stains mitochondria regardless of membrane potential) (Zhang, 1994) and CellMask™ Orange (for staining the plasma membrane) revealed that expanding BM-MSCs display a developed network composed of thread-like mitochondria spread throughout the cytoplasm (Fig. 2 (A)). Undifferentiated cells also display a mitochondrial population organized in a branched/reticulated network, yet we found a more fragmented morphology, mostly composed of rod-like particles, in differentiated cells. Quantitative analysis of mitochondrial morphology with the ImageJ software (De Vos and Sheetz, 2007) demonstrated, in differentiated cells, a decrease in the aspect ratio, which measures the elongation of mitochondrial particles, and an increased ratio of end points to branch points, which is inversely proportional to the mitochondrial networking (Fig. 2 (B)).

3.3. *Hepatogenic differentiation of BM-MSCs is accompanied by a mitochondrial biogenesis resulting in enhanced mitochondrial respiration*

BM-MSCs appear to display a more elongated and more developed mitochondrial network than the one reported in ESCs.

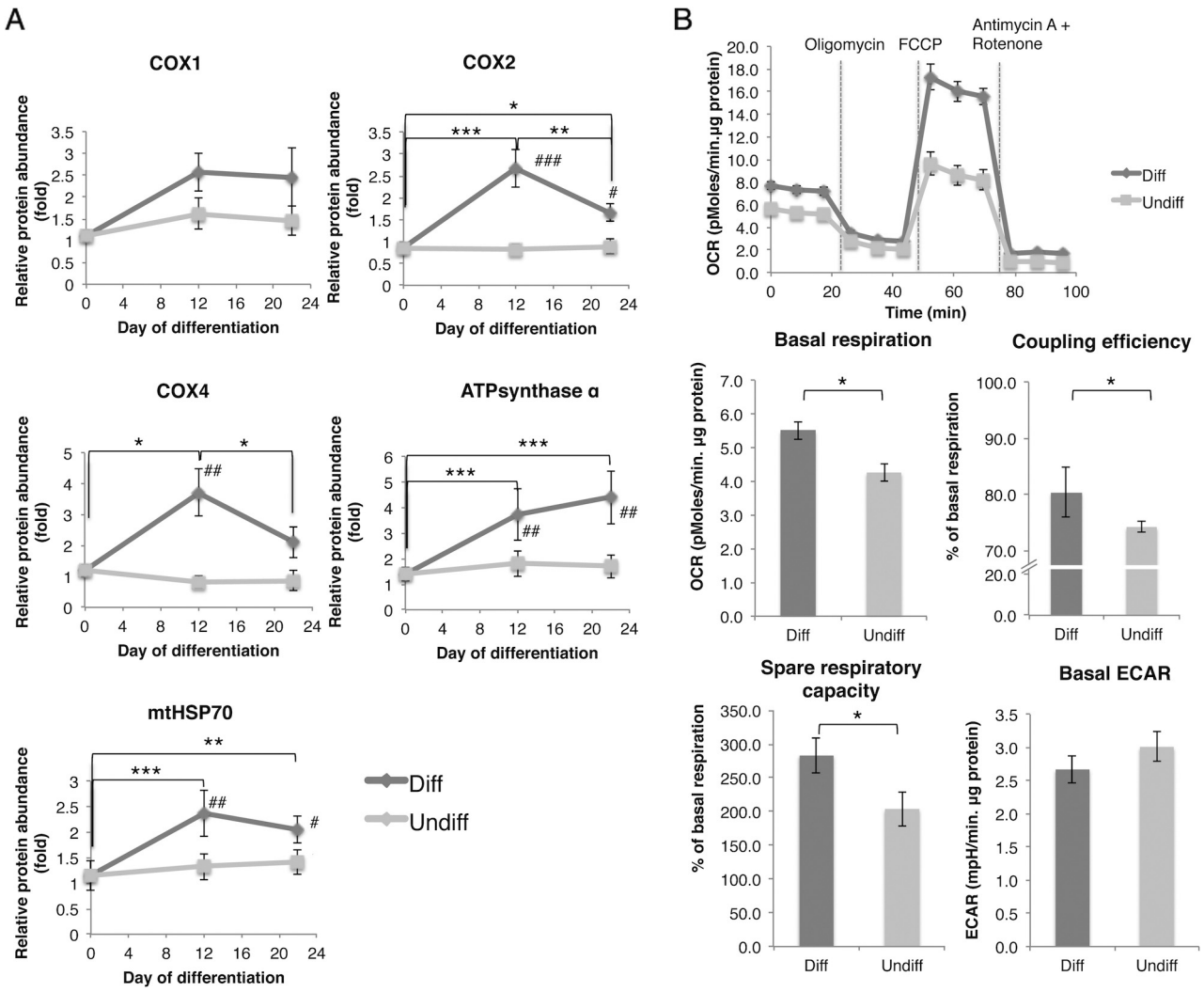

Fig. 4. An increase in several mitochondrial protein abundance and respiration is observed during the hepatogenic differentiation of BM-MSCs. (A): Relative abundance of several mitochondrial proteins was analyzed by Western-Blot. Signal intensity was quantified and normalized to the abundance of histone 3 (loading control). Data are presented as mean ± SEM ($n = 4$ independent donor cells). (B): OCR changes in response to oligomycin, FCCP and antimycin A in combination with rotenone were used to calculate the basal respiration, respiration coupling efficiency and spare respiratory capacity of differentiated and undifferentiated cells at day 12. The basal ECAR was also assessed. Data are presented as mean ± SEM ($n = 4$ independent donor cells).

Nevertheless, we hypothesized that both quantitative and qualitative changes in mitochondrial composition, perhaps driven by mitochondrial biogenesis regulators and leading to a metabolic shift toward increased OXPHOS, may accompany the hepatogenic differentiation of BM-MSCs. We thus first analyzed on immunofluorescence sections observed by confocal microscopy the fraction of cytoplasmic area occupied by mitochondria (Fig. 3 (A) and (D)). Interestingly, we evidenced a significant increase in the percentage of the cytoplasmic area occupied by mitochondria, rising from 11.23 ± 0.71% in expanding BM-MSCs, to 15.93 ± 1.25% and 16.32 ± 0.96% at the end of the hepatic induction and maturation steps respectively, while slightly decreasing in undifferentiated cells. We next analyzed the evolution of mtDNA copy number during the cell differentiation process. We observed a significant induction of mtDNA copy number in differentiating cells when compared with expanding BM-MSCs, reaching 2.13 ± 0.14 folds at the end of the induction step (day 12) and 3.87 ± 0.25 folds at the end of the maturation step (day 22). The mtDNA copy number remained stable in undifferentiated cells (Fig. 3 (B)). Although no change was found at the end of the hepatic induction step, we evidenced an increase in the relative number of nucleoids per cell at the end of the hepatic maturation step in differentiated cells (Fig. 3 (C) and (E)). Nevertheless, no significant difference was evidenced when considering the area density of nucleoids relative to mitochondria, which could be explained by a decreased size of nucleoids in differentiating cells when compared to expanding cells (Suppl. Fig. 2 (A) and (B)).

Given that mitochondrial biogenesis also requires the synthesis and import of many mitochondrial proteins, we next analyzed the abundance of several mitochondrial proteins throughout the differentiation process. The abundance of mtHSP70, a mitochondrial matrix chaperone required for the import and folding of most mitochondrial inner membrane and matrix proteins (Deocaris et al., 2006), although not significantly modified at the mRNA level (Suppl. Fig. 3) was found to be significantly induced at the protein level in differentiating cells (Fig. 4 (A)). In addition, the abundance of several proteins involved in the OXPHOS chain increased during the hepatogenic differentiation of BM-MSCs, both at the mRNA (Suppl. Fig. 3) and protein levels (Fig. 4 (A) and Suppl. Fig. 4). The protein abundance of the subunit II of the cytochrome c oxidase (COX2), which is encoded by mtDNA, was found to be significantly increased in differentiated cells (vs. expanding or undifferentiated BM-MSCs), with a maximum abundance reached at the end of the hepatogenic induction step (day 12). A comparable induction of

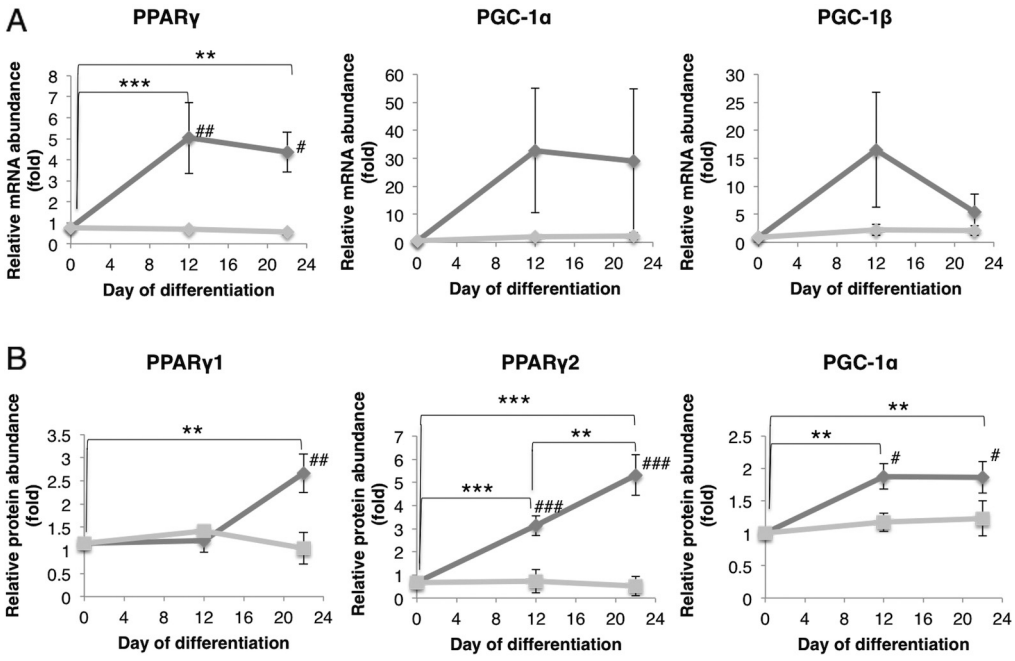

Fig. 5. An increased expression of several mitochondrial biogenesis regulators is observed during the hepatogenic differentiation of BM-MSCs. (A) PGC-1α, PGC-1β and PPARγ mRNA abundance was assessed by RT-qPCR. Data are presented as mean ± SEM (n = 4 independent donor cells). (B): Relative protein abundance was analyzed by Western-Blot. Signal intensity was quantified and normalized to the abundance of histone 3 (loading control). Data are presented as mean ± SEM (n = 4 independent donor cells).

the subunit IV (COX4, encoded by nDNA) occurred during the hepatogenic induction step, while the abundance of the subunit α of the ATP synthase increased continuously during the hepatogenic induction and maturation steps. While an increased abundance of the subunit I of the cytochrome c oxidase (COX1) (encoded by mtDNA) was also found in differentiating cells, the difference was not significant in our experimental conditions.

The increased abundance of several OXPHOS complex subunits prompted us to analyze the mitochondrial respiration at the end of the hepatogenic induction step. The OCR was thus measured in a basal condition after the addition of oligomycin A (an ATP synthase inhibitor, in order to evaluate the coupling efficiency of the respiratory chain), FCCP (an uncoupling protonophore, to evaluate the spare respiratory capacity of cells), and a combination of antimycin A and rotenone (mitochondrial complex III and I inhibitors, respectively). These conditions were necessary in order to calculate and subtract the non-mitochondrial oxygen consumption from other measurements (Brand and Nicholls, 2011) (Fig. 4 (B)). We found that the basal respiration was significantly increased in differentiated vs. undifferentiated cells, which suggests that differentiated cells rely more on OXPHOS for their ATP production. Moreover, the coupling efficiency, representing the fraction of the basal respiration that is used for ATP production, was significantly higher in differentiated cells. The spare respiratory capacity, which represents the cell's ability to increase substrates and electron flux across the OXPHOS chain to respond to an increased energy demand, was also higher in differentiated cells. Together, these data demonstrate that, in a basal condition, differentiated cells have a more efficient OXPHOS system and rely more on OXPHOS. Also, differentiated cells can increase their reliance on OXPHOS during increased energy demand. In addition to measuring the OCR, we also analyzed the ECAR in a basal condition. We observed a slightly lower ECAR in differentiated vs. undifferentiated cells, but the difference was not statistically significant. Altogether, these data strongly support a metabolic shift toward increased OXPHOS during the hepatogenic induction of BM-MSCs.

3.4. Several mitochondrial biogenesis regulators are increased during the hepatogenic differentiation of BM-MSCs

In order to investigate the potential mechanisms regulating the mitochondrial biogenesis in differentiating BM-MSCs, we analyzed the relative mRNA abundance of most of the well-known regulators of mitochondrial biogenesis. These regulators included PGC-1α, PGC-1β, PPARα, -γ and -δ, Nrf1 and Nrf2α, ERRα, POLG, POLG2, PolRmt, and TFAM at different time points of the differentiation process. Although no change was observed in the expression of most of these candidates (data not shown), we evidenced a trend toward an induction of the mRNA abundance of PPARγ (with no isoform discrimination) and of the global co-regulators PGC-1α and PGC-1β (Fig. 5 (A)). At the protein level, we observed a significant induction of PPARγ1 at the end of the differentiation, and of both PPARγ2 and PGC-1α at the end of the induction and maturation steps (Fig. 5 (B)). Together with the previous results, these data further support that an enhanced mitochondrial biogenesis process occurs during the hepatogenic differentiation of BM-MSCs. This process involves at least two well-known regulators of mitochondrial biogenesis and results in the replication of mtDNA, synthesis of mitochondrial proteins and increased mitochondrial respiration.

3.5. Mitochondrial modifications occur during the in vitro dedifferentiation of human primary hepatocytes

The reprogramming of somatic cells into iPSCs correlates with a reduction of mitochondrial abundance and function, a remodeling of which is required for the induction of pluripotency in iPSCs (Xu et al., 2013). We thus aimed to determine if similar structural or functional remodeling of mitochondria occurs during the spontaneous *in vitro* dedifferentiation of hepatocytes, in order to evidence reverse mitochondrial changes correlating with hepatocyte (de-)differentiation.

A drastic loss of multiple hepatic gene markers, including albumin (p = 0.055), glucose-6-phosphatase (G6PC) (p = 0.054),

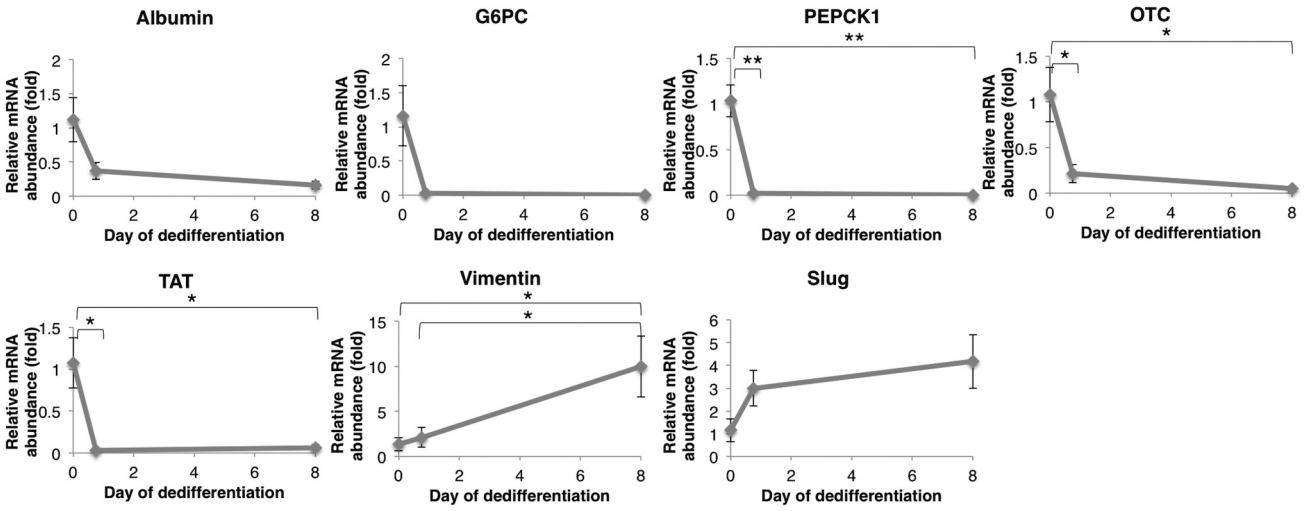

Fig. 6. Primary human hepatocyte dedifferentiation is associated with the rapid loss of hepatic (albumin, G6PC, PEPCK1, OTC, TAT) and progressive acquisition of mesenchymal markers (vimentin, snail). mRNA abundance was assessed by RT-qPCR. Data are presented as mean ± SEM ($n = 3$ independent donor cells).

phosphoenolpyruvate carboxykinase 1 (PEPCK1), ornithine transcarbamylase (OTC) and tyrosine amino-transferase (TAT) was noted within 18 h post-isolation at the mRNA level (Fig. 6). Regarding mesenchymal markers (which are induced during the spontaneous *in vitro* dedifferentiation of hepatocytes (Meyer, Dzieran, 2013), a statistically significant induction of vimentin, along with a moderate increase in the abundance of slug, were observed at the mRNA level (Fig. 6).

Interestingly, the analysis of the mitochondrial morphology throughout the dedifferentiation process exhibited changes to the network structure that were the opposite of those observed in the differentiation model (Fig. 7 (A)). Indeed, the mitochondrial aspect ratio increased, while the ratio of end points to branch points decreased during the dedifferentiation process (Fig. 7 (B)), which supports an elongation and increased networking of mitochondria. In addition, we found a repression of the abundance of several OXPHOS complex subunits heretofore demonstrated to be induced in the differentiation model: COX1, COX2, COX4, and the subunit α of the ATP synthase (Fig. 7 (C) and Suppl. Fig. 5). These data suggest that opposite changes in the mitochondrial network morphology, and in the abundance of proteins involved in mitochondrial activity, occur during the differentiation of BM-MSCs into hepatocyte-like cells and in the dedifferentiation of primary hepatocytes.

4. Discussion

Recent discoveries have demonstrated a strong interplay between mitochondrial biogenesis/function and stemness/differentiation programs in ESCs and iPSCs. However, evidence of a similar phenomenon in MSCs is (to our knowledge) very scarce, and limited to the contexts of osteogenic (Chen, Shih, 2008, Palomaki, Pietila, 2013, Pietila et al., 2010, Pietila, Palomaki, 2012) and adipogenic (Hofmann et al., 2012, Huang, Chen, 2011, Tormos, Anso, 2011) differentiation. It is still unclear whether this phenomenon is a hallmark of cell differentiation programs, or displays specificities depending on the stem cell types or lineages into which they are differentiated. Investigation of multiple models is therefore required. In this study we provide, for the first time, a detailed characterization of the mitochondrial changes occurring during the hepatogenic differentiation of BM-MSCs. We first evidenced an increased mitochondria to cytoplasm ratio, suggesting that the cytoplasm of differentiating cells is enriched in mitochondria compared to expanding or undifferentiating cells. The induction of mtDNA abundance during the hepatogenic differentiation (3.87 folds) appeared stronger than during the osteogenic differentiation of BM-MSCs (1.37 folds) (Chen, Shih, 2008) and resulted at the end of the hepatic maturation step in an increased number of nucleoids. Nevertheless, we did not find any significant change in the area density of nucleoids when normalized to the mitochondrial content (Suppl. Fig. 2(A)), which can be explained both by an increase in mitochondrial content as well as by a decrease in nucleoid size (Suppl. Fig. 2(B)). This decrease in nucleoid size both in differentiated and undifferentiated cells versus expanding cells might be explained by the serum withdrawal in those conditions, as the serum deprivation has been associated with more condensed nucleoids (Prachar, 2010). Obviously this nucleoid compaction does not impact mtDNA-encoded gene expression, as both COX1 and COX2 are similarly expressed in expanding and undifferentiated BM-MSCs (Suppl. Fig. 3).

In addition to the increase in mtDNA, we observed (as already demonstrated during the osteogenic (Chen, Shih, 2008) and adipogenic (Hofmann, Beyer, 2012) differentiation of BM-MSCs) an increased expression for several mitochondrial proteins, including OXPHOS subunits. Although the mitochondrial chaperone mtHSP70 is upregulated at the post-transcriptional level only, we evidenced an increased mRNA abundance for COX1, COX2, COX4i1 and ATP5A1. Interestingly, the mRNA levels of nDNA-encoded subunits (COX4i1 and ATP5A1) were induced to a lesser extent than the protein levels, while similar mRNA and protein induction folds were found for mtDNA-encoded subunits. These data suggest that nDNA-encoded and mtDNA-encoded subunit expression is upregulated by different mechanisms to finally reach an increased and balanced production of OXPHOS complexes.

Although we found a continuous increase in the mtDNA abundance and a still significantly increased abundance in several mitochondrial proteins and biogenesis regulators at the end of the hepatogenic maturation step (day 22), we did notice a peak in the abundance of several mitochondrial proteins at the end of the induction step (day 12). These data suggest that the mtDNA copy number is not necessarily associated with OXPHOS subunit expression, which is in agreement with data showing that mtDNA is not correlated with the cytochrome c oxidase activity in different cell types (Van den Bogert et al., 1993). The different constituent of mitochondria (lipids, mtDNA and proteins) might therefore be differentially regulated. Interestingly, studies of adipogenic or osteogenic differentiation of BM-MSCs also evidenced an increase in mitochondrial biogenesis and function during the early steps

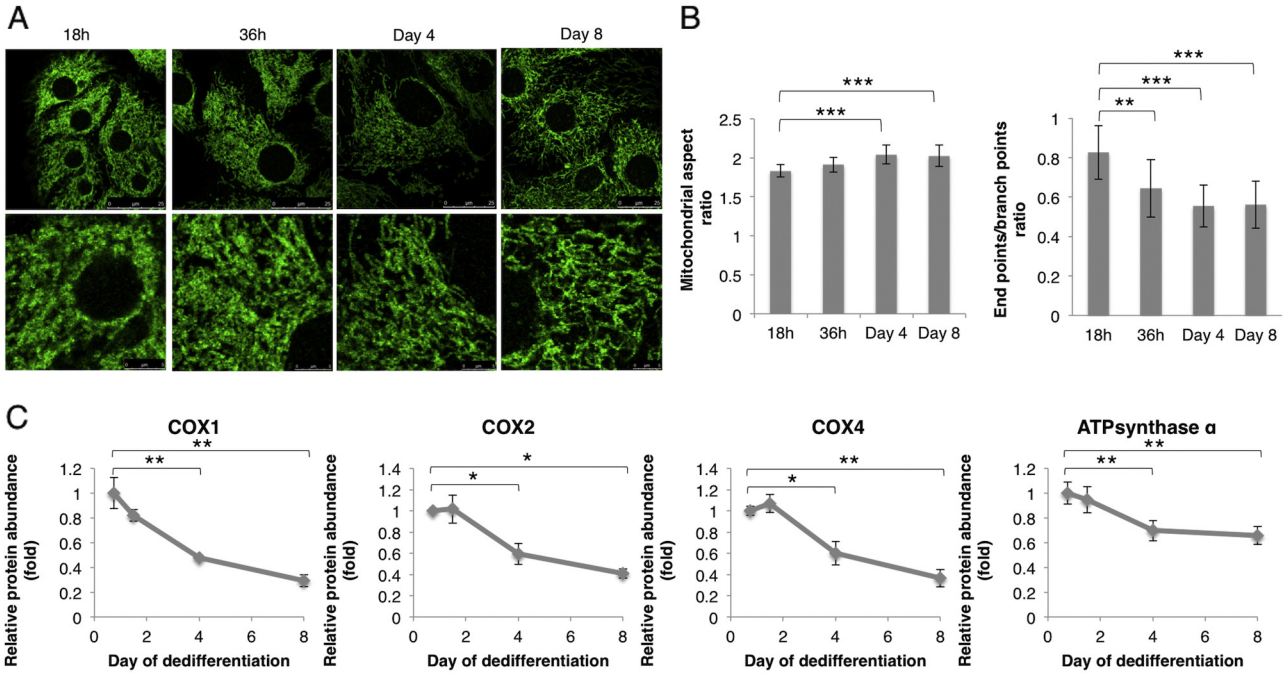

Fig. 7. Opposite changes in the mitochondrial network morphology and OXPHOS protein abundance are observed in dedifferentiating primary hepatocytes. (A) The mitochondrial network morphology was visualized by performing a TOM20 immunofluorescence combined with confocal microscopy visualization. (B): The aspect ratio and end points/branch points ratio were analyzed for 12 cells for each time-point of the dedifferentiation process. Data are presented as mean ± standard deviation. (C). Relative abundance of several mitochondrial proteins was analyzed by Western-Blot. Signal intensity was quantified and normalized to the abundance of histone 3 (loading control). Data are presented as mean ± SEM ($n = 3$ independent donor cells) and expressed relative to the 18 h time point.

of the differentiation process (Chen, Shih, 2008, Pietila, Palomaki, 2012, Tormos, Anso, 2011). It remains to be determined whether this increased mitochondrial abundance and activity, which precedes the hepatogenic maturation in our model, is important for the commitment and early induction of differentiation, and/or if the continuous increase in mtDNA and mitochondrial abundance are also required for the late differentiation stages.

At the functional level, we demonstrated an increased oxidative activity (basal respiration), capacity (respiratory reserve), and efficiency (coupling efficiency) of differentiating cells. Therefore, both quantitative and qualitative modifications of the mitochondrial network occurred during the hepatogenic differentiation of BM-MSCs, resulting in enhanced mitochondrial respiration. We next evidenced an increased expression of the co-activator PGC-1α (Fig. 5), considered a key regulator of mitochondrial biogenesis and oxidative metabolism (Scarpulla, 2011). We also found an induction of PPARγ both during the steps of hepatogenic induction (isoform 2) and maturation (both isoforms). Interestingly, these data are consistent with the previously described PPARγ-dependent induction of PGC-1α and -β expression (Deng et al., 2011, Hondares et al., 2006). These co-regulators may in turn drive the mitochondrial biogenesis process and oxidative switch by co-activating the many TFs that regulate mitochondrial gene expression.

The interest devoted to mitochondrial abundance and activity in stemness and differentiation results from the relevance conferred by observations made in multiple models (diverse stem cells and differentiation types (Chen, Hsu, 2012, Xu et al., 2013)). Yet there is also the intriguing fact that opposite modifications occur during the reprogramming of somatic cells into iPSCs (Xu et al., 2013). This process has been, so far, only demonstrated in the artificial context of genetically-engineered reprogramming. In this study, we took advantage of the spontaneous dedifferentiation process occurring during primary hepatocytes *in vitro* culture to test whether opposite changes are observed during hepatic differentiation and dedifferentiation.

Interestingly, we evidenced a decreased abundance in several OXPHOS protein subunits (Fig. 7 (C)), all of which were induced in the BM-MSCs hepatogenic differentiation model (Fig. 4 (A)). Importantly, the spontaneous dedifferentiation process of hepatocytes does not lead to the re-establishment of pluripotency like in iPSC reprogramming. Our data therefore suggest that the diminished mitochondrial OXPHOS subunit abundance is observed as soon as cells are loosing their fully differentiated phenotype, and do not require the re-acquisition of pluripotency. Although this would require validation in other models, these data might suggest that mitochondria are remodeled throughout the kinetics of differentiation/dedifferentiation programs and not involved in a time-limited switch between pluripotency and commitment to a differentiation program.

BM-MSCs display tubular interconnected mitochondria spread throughout the cytoplasm. While ESCs are generally reported to display granular mitochondria (although some discrepancies exist, depending on the studies) (Lonergan et al., 2006, Mandal, Lindgren, 2011, Sathananthan et al., 2002, St John, Ramalho-Santos, 2005), we observed in human umbilical cord-derived MSCs, as well as in adult human liver mesenchymal stem/progenitor cells, a more comparable mitochondrial morphology than in BM-MSCs (unpublished data). This developed tubular mitochondrial network may thus be typical of mesenchymal stem/progenitor cells. During hepatogenic differentiation, the mitochondrial network of BM-MSCs undergoes a fragmentation, leading to smaller mitochondria. The reasons for these modifications in the mitochondrial network morphology during hepatogenic differentiation are still unknown. However, several hypotheses may partly explain these changes. First, an increasing number of studies point toward an involvement of mitochondrial fusion/fission processes in cell proliferation and differentiation programs. As recently reviewed by Mitra (Mitra, 2013), multiple evidence supports the hypothesis that a reduced expression or activity of dynamin-related protein 1 (Drp1, involved in the mitochondrial fission machinery) results in unopposed

mitochondrial fusion and promotes cell proliferation through the build-up of cyclin E, which regulates the entry in the S-phase of the cell cycle. The highly fused mitochondrial network of expanding BM-MSCs (Fig. 2) may therefore partly reflect the proliferation status of these cells. In addition, we observed the progressive acquisition of a slightly more fused mitochondrial network during the dedifferentiation of hepatocytes (Fig. 7 (A) and (B)). Since isolated hepatocytes re-enter proliferation during isolation and *in vitro* culture (Elaut, Henkens, 2006), this hypothesis may also partly explain the increased branching and elongation of mitochondria during early dedifferentiation. Secondly, it has been suggested that mitochondrial dynamics influence OXPHOS capacity (Benard et al., 2010). For instance, it has been demonstrated that inhibiting mitochondrial fission, through down-regulating Drp1 expression, results in decreased mtDNA abundance and OXPHOS activity (Parone et al., 2008). Conversely, OXPHOS activity is also reported to influence mitochondrial dynamics (Benard, Bellance, 2010). Therefore, the modifications of the mitochondrial network morphology of differentiating BM-MSCs may represent a prerequisite (or a consequence) of the observed increased OXPHOS activity. Thirdly, the opposite modifications in mitochondrial network morphology may result from changes in cytoskeleton structure during the hepatic differentiation and dedifferentiation processes. Indeed, we found an important decrease in β-actin and α-tubulin abundance during the differentiation of BM-MSCs, while a strong induction of these proteins was observed during the dedifferentiation of hepatocytes (data not shown). Interestingly, mitochondrial location, shape, and tubular status are known to be regulated through their interaction with, and modification of, shape proteins and cytoskeleton elements (such as the microtubules, microfilaments, and intermediary filament families), resulting in changes in mitochondrial morphology (Kuznetsov et al., 2009).

5. Conclusion

While we observed a fragmentation of the mitochondrial network morphology and an induction of mitochondrial biogenesis and activity during the hepatogenic differentiation of BM-MSCs, we reported several opposite changes during the spontaneous dedifferentiation of primary hepatocytes. These observations support the hypothesis of a strong involvement of mitochondria and mitochondrial metabolism in regulating the differentiation of stem cells and dedifferentiation or reprogramming events. Further research is still required to unravel the mechanisms involved in the interplay between these two processes. Understanding how these processes are regulated, and determining if they regulate each other, is of great interest for the improvement of directed differentiation of stem cells into specific cell types. Even though there is continuous improvement of their efficiency, current differentiation protocols do not enable one to reach a terminal differentiation status as observed in primary somatic cells. This is particularly true in the context of hepatic differentiation, in which even the most efficient protocols do not allow for reaching similar levels of hepatic functions, or inducing all hepatic activities simultaneously (Zhang et al., 2013, Zhou et al., 2012). On the other hand, understanding how opposite mitochondrial modifications occur during primary hepatocyte dedifferentiation may, in turn, help to preserve them in a more differentiated status. Understanding the role played by mitochondria in hepatic differentiation and dedifferentiation may therefore be useful in regenerative medicine and pharmacological testing.

Conflicts of interest

The authors declare no conflict of interest

Acknowledgments

Anaïs Wanet is a recipient of the FNRS fellowship (Fonds National de la Recherche Scientifique, Belgium). The authors thank Pr. Sonveaux group and particularly Paolo Porporato (FATH, IREC, Université Catholique de Louvain, Brussels, Belgium) for their help with respiration analyses, as well as Antoine Fattaccioli, Aude Sauvage, Catherine Demazy and Noëlle Ninane (URBC, University of Namur, Belgium) for technical support.

Appendix A. Supplementary data

Supplementary data associated with this article can be found, in the online version, at http://dx.doi.org/10.1016/j.biocel.2014.07.015.

References

Banas A, Yamamoto Y, Teratani T, Ochiya T. Stem cell plasticity: learning from hepatogenic differentiation strategies. Developmental Dynamics: An Official Publication of the American Association of Anatomists 2007;236:3228–41.
Benard G, Bellance N, Jose C, Melser S, Nouette-Gaulain K, Rossignol R. Multi-site control and regulation of mitochondrial energy production. Biochimica et Biophysica Acta 2010;1797:698–709.
Brand MD, Nicholls DG. Assessing mitochondrial dysfunction in cells. The Biochemical Journal 2011;435:297–312.
Chen CT, Hsu SH, Wei YH. Mitochondrial bioenergetic function and metabolic plasticity in stem cell differentiation and cellular reprogramming. Biochimica et Biophysica Acta 2012;1820:571–6.
Chen CT, Shih YR, Kuo TK, Lee OK, Wei YH. Coordinated changes of mitochondrial biogenesis and antioxidant enzymes during osteogenic differentiation of human mesenchymal stem cells. Stem Cells 2008;26:960–8.
Cho YM, Kwon S, Pak YK, Seol HW, Choi YM, Park do J, et al. Dynamic changes in mitochondrial biogenesis and antioxidant enzymes during the spontaneous differentiation of human embryonic stem cells. Biochemical and Biophysical Research Communications 2006;348:1472–8.
Chung S, Arrell DK, Faustino RS, Terzic A, Dzeja PP. Glycolytic network restructuring integral to the energetics of embryonic stem cell cardiac differentiation. Journal of Molecular and Cellular Cardiology 2010;48:725–34.
De Vos KJ, Sheetz MP. Visualization and quantification of mitochondrial dynamics in living animal cells. Methods in Cell Biology 2007;80:627–82.
Deng T, Sieglaff DH, Zhang A, Lyon CJ, Ayers SD, Cvoro A, et al. A peroxisome proliferator-activated receptor gamma (PPARgamma)/PPARgamma coactivator 1beta autoregulatory loop in adipocyte mitochondrial function. The Journal of Biological Chemistry 2011;286:30723–31.
Deocaris CC, Kaul SC, Wadhwa R. On the brotherhood of the mitochondrial chaperones mortalin and heat shock protein 60. Cell Stress & Chaperones 2006;11:116–28.
Elaut G, Henkens T, Papeleu P, Snykers S, Vinken M, Vanhaecke T, et al. Molecular mechanisms underlying the dedifferentiation process of isolated hepatocytes and their cultures. Current Drug Metabolism 2006;7:629–60.
Facucho-Oliveira JM, Alderson J, Spikings EC, Egginton S. St John JC. Mitochondrial DNA replication during differentiation of murine embryonic stem cells. Journal of Cell Science 2007;120:4025–34.
Fernandez-Marcos PJ, Auwerx J. Regulation of PGC-1alpha, a nodal regulator of mitochondrial biogenesis. The American Journal of Clinical Nutrition 2011;93:884S–90S.
Folmes CD, Nelson TJ, Martinez-Fernandez A, Arrell DK, Lindor JZ, Dzeja PP, et al. Somatic oxidative bioenergetics transitions into pluripotency-dependent glycolysis to facilitate nuclear reprogramming. Cell Metabolism 2011;14:264–71.
Hock MB, Kralli A. Transcriptional control of mitochondrial biogenesis and function. Annual Review of Physiology 2009;71:177–203.
Hofmann AD, Beyer M, Krause-Buchholz U, Wobus M, Bornhauser M, Rodel G. OXPHOS supercomplexes as a hallmark of the mitochondrial phenotype of adipogenic differentiated human MSCs. PloS One 2012;7:e35160.
Hondares E, Mora O, Yubero P, Rodriguez de la Concepcion M, Iglesias R, Giralt M, et al. Thiazolidinediones and rexinoids induce peroxisome proliferator-activated receptor-coactivator (PGC)-1alpha gene transcription: an autoregulatory loop controls PGC-1alpha expression in adipocytes via peroxisome proliferator-activated receptor-gamma coactivation. Endocrinology 2006;147:2829–38.
Huang PI, Chen YC, Chen LH, Juan CC, Ku HH, Wang ST, et al. PGC-1alpha mediates differentiation of mesenchymal stem cells to brown adipose cells. Journal of Atherosclerosis and Thrombosis 2011;18:966–80.
Kuznetsov AV, Hermann M, Saks V, Hengster P, Margreiter R. The cell-type specificity of mitochondrial dynamics. The International Journal of Biochemistry & Cell Biology 2009;41:1928–39.
Lonergan T, Bavister B, Brenner C. Mitochondria in stem cells. Mitochondrion 2007;7:289–96.

Lonergan T, Brenner C, Bavister B. Differentiation-related changes in mitochondrial properties as indicators of stem cell competence. Journal of Cellular Physiology 2006;208:149–53.
Mandal S, Lindgren AG, Srivastava AS, Clark AT, Banerjee U. Mitochondrial function controls proliferation and early differentiation potential of embryonic stem cells. Stem Cells 2011;29:486–95.
Meyer C, Dzieran J, Liu Y, Schindler F, Munker S, Muller A, et al. Distinct dedifferentiation processes affect caveolin-1 expression in hepatocytes. Cell Communication and Signaling: CCS 2013;11:6.
Mitra K. Mitochondrial fission-fusion as an emerging key regulator of cell proliferation and differentiation. BioEssays: News and Reviews in Molecular, Cellular and Developmental Biology 2013;35:955–64.
Mosna F, Sensebe L, Krampera M. Human bone marrow and adipose tissue mesenchymal stem cells: a user's guide. Stem Cells and Development 2010;19:1449–70.
Najar M, Raicevic G, Fayyad-Kazan H, De Bruyn C, Bron D, Toungouz M, et al. Impact of different mesenchymal stromal cell types on T-cell activation, proliferation and migration. International Immunopharmacology 2013;15:693–702.
Najimi M, Khuu DN, Lysy PA, Jazouli N, Abarca J, Sempoux C, et al. Adult-derived human liver mesenchymal-like cells as a potential progenitor reservoir of hepatocytes. Cell Transplantation 2007;16:717–28.
Palomaki S, Pietila M, Laitinen S, Pesala J, Sormunen R, Lehenkari P, et al. HIF-1alpha is upregulated in human mesenchymal stem cells. Stem Cells 2013;31:1902–9.
Parone PA, Da Cruz S, Tondera D, Mattenberger Y, James DI, Maechler P, et al. Preventing mitochondrial fission impairs mitochondrial function and leads to loss of mitochondrial DNA. PloS One 2008;3:e3257.
Pietila M, Lehtonen S, Narhi M, Hassinen IE, Leskela HV, Aranko K, et al. Mitochondrial function determines the viability and osteogenic potency of human mesenchymal stem cells. Tissue Engineering Part C, Methods 2010;16:435–45.
Pietila M, Palomaki S, Lehtonen S, Ritamo I, Valmu L, Nystedt J, et al. Mitochondrial function and energy metabolism in umbilical cord blood- and bone marrow-derived mesenchymal stem cells. Stem Cells and Development 2012;21:575–88.
Prachar J. Mouse and human mitochondrial nucleoid–detailed structure in relation to function. General Physiology and Biophysics 2010;29:160–74.
Prigione A, Fauler B, Lurz R, Lehrach H, Adjaye J. The senescence-related mitochondrial/oxidative stress pathway is repressed in human induced pluripotent stem cells. Stem Cells 2010;28:721–33.
Sathananthan H, Pera M, Trounson A. The fine structure of human embryonic stem cells. Reproductive Biomedicine Online 2002;4:56–61.
Scarpulla RC. Metabolic control of mitochondrial biogenesis through the PGC-1 family regulatory network. Biochimica et Biophysica Acta 2011;1813:1269–78.
St John JC, Ramalho-Santos J, Gray HL, Petrosko P, Rawe VY, Navara CS, et al. The expression of mitochondrial DNA transcription factors during early cardiomyocyte in vitro differentiation from human embryonic stem cells. Cloning and Stem Cells 2005;7:141–53.
Suhr ST, Chang EA, Tjong J, Alcasid N, Perkins GA, Goissis MD, et al. Mitochondrial rejuvenation after induced pluripotency. PloS One 2010;5:e14095.
Tormos KV, Anso E, Hamanaka RB, Eisenbart J, Joseph J, Kalyanaraman B, et al. Mitochondrial complex III ROS regulate adipocyte differentiation. Cell Metabolism 2011;14:537–44.
Van den Bogert C, De Vries H, Holtrop M, Muus P, Dekker HL, Van Galen MJ, et al. Regulation of the expression of mitochondrial proteins: relationship between mtDNA copy number and cytochrome-c oxidase activity in human cells and tissues. Biochimica et Biophysica Acta 1993;1144:177–83.
Varum S, Rodrigues AS, Moura MB, Momcilovic O, At Easley C, Ramalho-Santos J, et al. Energy metabolism in human pluripotent stem cells and their differentiated counterparts. PloS One 2011;6:e20914.
Xu X, Duan S, Yi F, Ocampo A, Liu GH. Izpisua Belmonte JC. Mitochondrial regulation in pluripotent stem cells. Cell Metabolism 2013;18:325–32.
Zhang YZ. Novel fluorescent acidic organelle-selective dyes and Mitochondrion-selective dyes that are well retained during cell fixation and permeabilization. Molecular Biology of the Cell 1994;5:113–653.
Zhang Z, Liu J, Liu Y, Li Z, Gao WQ, He Z. Generation, characterization and potential therapeutic applications of mature and functional hepatocytes from stem cells. Journal of Cellular Physiology 2013;228:298–305.
Zhou WL, Medine CN, Zhu L, Hay DC. Stem cell differentiation and human liver disease. World Journal of Gastroenterology: WJG 2012;18:2018–25.